HHS Public Access

Author manuscript

NMR Biomed. Author manuscript; available in PMC 2023 September 28.

Published in final edited form as:

NMR Biomed. 2017 August ; 30(8): . doi:10.1002/nbm.3733.

Regional Quantification of Myocardial Mechanics in Rat using 3D cine DENSE Cardiovascular Magnetic Resonance

Xiaoyan Zhang[1,†], **Zhan-Qiu Liu**[1,†], **Dara Singh**[1], **Gregory J. Wehner**[2], **David K. Powell**[3], **Kenneth S. Campbell**[4], **Brandon K. Fornwalt**[2,4,5], **Jonathan F. Wenk**[1,6,*]

[1]Department of Mechanical Engineering, University of Kentucky, Lexington, KY, USA

[2]Department of Biomedical Engineering, University of Kentucky, Lexington, KY, USA

[3]Department of Anatomy and Neurobiology, University of Kentucky, Lexington, KY, USA

[4]Department of Physiology, University of Kentucky, Lexington, KY, USA

[5]Institute for Advanced Application, Geisinger Health System, Danville, PA

[6]Department of Surgery, University of Kentucky, Lexington, KY, USA

Abstract

Rat models have assumed an increasingly important role in cardiac research. However, a detailed profile of regional cardiac mechanics, such as strains and torsion, is lacking in rats. We hypothesized that healthy rat left ventricles (LV) exhibit regional differences in cardiac mechanics, which are part of normal function. In this study, images of the LV were obtained with 3D cine displacement encoding with stimulated echoes (DENSE) cardiovascular magnetic resonance (CMR) in 10 healthy rats. To evaluate regional cardiac mechanics, the LV was divided into basal, mid-ventricular, and apical regions. The myocardium at the mid-LV was further partitioned into four wall segments (i.e., septal, inferior, lateral, and anterior) and three transmural layers (i.e., sub-endocardium, mid-myocardium, and sub-epicardium). The 6 Lagrangian strain components (i.e., E_{rr}, E_{cc}, E_{ll}, E_{cl}, E_{rl}, and E_{cr}) were computed from the 3D displacement field and averaged within each region of interest. Torsion was quantified using the circumferential-longitudinal shear angle. While peak systolic E_{cl} differed between the mid-ventricle and apex, the other 5 components of peak systolic strain were similar across the base, mid-ventricle, and apex. In the mid-LV myocardium, E_{cc} decreased gradually from the sub-endocardial to the sub-epicardial layer. E_{ll} demonstrated significant differences between the four wall segments with the largest magnitude in the inferior segment. E_{rr} was uniform among the four wall segments. E_{cl} varied along the transmural direction and among wall segments, whereas E_{rl} differed only among the wall segments. E_{rc} was not associated with significant variations. Torsion also varied along the transmural direction and among wall segments. These results provide fundamental insights into the regional contractile function of healthy rat hearts, and form the foundation for future studies on regional changes induced by disease or treatments.

[*]**Corresponding Author:** Jonathan F. Wenk, PhD, University of Kentucky, Department of Mechanical Engineering, 269 Ralph G. Anderson Building, Lexington, KY, 40506, Phone: (859) 218-0658, Fax: (859) 257-3304, wenk@engr.uky.edu.
[†]These authors contributed equally to this work.

Keywords

3D cine DENSE CMR; strain; torsion; rat

INTRODUCTION

Rat models have been increasingly used in cardiac research to better understand the progression of heart disease, including myocardial infarction and age-associated heart failure [1–3]. Previous studies have reported transmural differences in ventricular mechanics during disease development [4–7], which were linked to adverse changes in cardiac output and dyssynchrony. In addition, it has been shown that ventricular myocardium from different regions of the heart respond differently to pharmacological treatments [5]. These findings highlight the need for accurate normative data (including 3D strain and ventricular torsion) in order to assess regional changes in cardiac performance due to disease and treatment. Since this information is currently lacking for rat models, a detailed characterization of normal cardiac mechanics in the left ventricle (LV) of healthy rats, therefore, is of considerable importance.

Cardiovascular magnetic resonance (CMR) has emerged as the gold standard method for non-invasively tracking LV motion. Compared to other common non-invasive methods, such as echocardiography, CMR is generally considered to be more accurate and reproducible [8]. With cine imaging and tissue tracking methods, CMR is able to quantify not only the LV volume, stroke volume, ejection fraction, and wall thickening, but also the myocardial strain, twist, and torsion [9]. Current CMR tissue tracking methods include myocardial tagging [10], harmonic phase analysis (HARP) [11], velocity encoded phase contrast [12], and displacement encoding with stimulated echoes (DENSE) [13, 14]. Previous studies have measured principal strains and/or torsion in normal healthy rats using HARP and DENSE, respectively [15, 16]. Results from these studies, however, were in 2 dimensions. Moreover, detailed transmural patterns of cardiac mechanics, especially at the mid-ventricle, were neglected in these studies.

In the present study, we hypothesized that healthy rat LVs exhibit regional differences in cardiac mechanics. For this purpose, 3D cine DENSE CMR, which provides the advantages of high strain resolution, high displacement accuracy, and rapid post-processing, was performed to quantify the regional distribution of 3D myocardial mechanics (i.e., Lagrangian strains and ventricular torsion) in healthy rat LVs. Inter-observer reproducibility was also quantified. The results of the present study provide fundamental insights into regional contractile function of the LV myocardium in rats, which is currently lacking in the literature, and will facilitate future experimental and computational investigation of heart disease in rat models.

METHODS

Animal preparation

10 female Sprague-Dawley rats (~6 months; Harlan) were used in this study. Animals were anesthetized with 2.5% isoflurane in oxygen at a rate of 1.5 L/min. Cutaneous ECG electrodes were placed on three legs for cardiac gating. Respiratory gating was performed with a respiratory sensor placed underneath the abdomen. Body temperature was monitored with a rectal thermometer and maintained at 36±1 °C with a customized heating pad. All vital signs including heart rate (334±7 beats per minute), respiratory rate (32±2 per minute) and body temperature were monitored with a fiber optic system (SA Instruments, Inc, Stony Brook, NY). All animal procedures were approved by the Institutional Animal Care and Use Committee at the University of Kentucky and were in agreement with the National Institute of Health's guidelines for the care and use of laboratory animals (NIH Publication 85–23, revised 1996).

CMR image acquisition

CMR was performed on a 7-Tesla Bruker ClinScan system (Bruker, Ettlingen, Germany) equipped with a 2 × 2 hydrogen phased-array coil and a gradient system (strength: 450 mT/m; slew rate: 4500 T/m/s). Multi-slice 3D encoded spiral cine DENSE (i.e., 3D cine DENSE) CMR was performed for image acquisition as described previously [9, 17]. Briefly, immediately following an ECG R-wave trigger detection, a displacement encoding module, which consists of radiofrequency and gradient pulses, was applied to store position-encoded longitudinal magnetization. This was followed by successive applications of a readout module, which employed a radiofrequency excitation pulse (constant flip angle = 20 degrees), a displacement un-encoding gradient, and an interleaved spiral k-space trajectory. As a result, a magnitude image was constructed and three phase images were independently encoded for 'x', 'y', and 'z' displacements, respectively, at each frame (Figure 1) via balanced encoding [18]. For each animal, a total of 17–22 frames per cardiac cycle were collected using both cardiac and respiratory gating with a repetition time of 7.4 ms and an echo time of 1 ms. Other relevant acquisition parameters included: pixel size = 0.357 × 0.357 mm, field of view = 50 × 50 mm, slice thickness = 1.3 mm, spiral interleaves = 36, and displacement encoding frequency = 0.3 cycles/mm.

To consistently visualize the majority of the LV wall throughout the entire cardiac cycle, 5–6 short-axis slices without slice gaps were defined, depending on the ventricular size, at end systole (ES) to cover approximately 80% of end-systolic ventricular length. Both 4-chamber and 2-chamber long-axis images were also acquired. The average acquisition time of 3D cine DENSE CMR images was around 30 minutes for each animal.

Image analysis

The displacement-encoded phase images were analyzed offline using *DENSEanalysis*, an open-source application available at www.denseanalysis.com [19, 20] that has been used to investigate the 3D myocardial mechanics in mice [9]. The myocardium was segmented from the blood pool and surrounding tissue using a semi-automated motion-guided segmentation method [21], for which manual correction was performed as needed. It should be noted

that the papillary muscles were identified and excluded from myocardial contours by displaying the short-axis contours in the long-axis images. Moreover, the abnormal segments of myocardial contours caused by noise in the phase images were also marked and excluded from the strain calculation. Following semi-automatic phase unwrapping, 3D displacement of each pixel throughout the cardiac cycle was derived with a tissue tracking technique [9, 20]. The components of the 3D Lagrangian finite strain tensor were derived in polar coordinates, relative to the referential frame at end diastole (ED; i.e., the first time frame), which consisted of 6 components: radial strain E_{rr}, circumferential strain E_{cc}, longitudinal strain E_{ll}, and 3 shear strains (E_{cl}, E_{rl}, and E_{cr}) [9]. Details related to the calculation of the displacement field, deformation gradient tensor, and Lagrangian strain tensor are provided in [9, 19].

Left ventricular torsion was represented as the circumferential-longitudinal (CL) shear angle α_{CL} between the basal and apical slices from ED to the time point of interest, and was computed using 3 strain components as follows [22]:

$$\alpha_{CL} = \sin^{-1}\frac{2E_{cl}}{\sqrt{(1+2E_{cc})(1+2E_{ll})}},$$

In order to evaluate the regional distribution of cardiac mechanics, the ventricle was initially divided into basal, mid-ventricular, and apical regions. For a more in-depth analysis, the myocardium at the mid-LV was divided into four wall segments (i.e., septal, inferior, lateral, and anterior segments) (Figure 2). Specifically, the septum was identified as the segment between the two right ventricular insertion points; the remaining wall was then divided into thirds for the other three regions. Moreover, each segment was partitioned equally into three transmural layers (i.e., sub-endocardium, mid-myocardium, and sub-epicardium). The strain and CL shear angle were then averaged within each region of interest. All of the regional segmenting was performed in *DENSEanalysis*, which allowed for the partitioning of the LV in the longitudinal, circumferential, and transmural directions.

Reproducibility assessment

Inter-observer reproducibility was performed as previously described [17]. Briefly, a second investigator analyzed the same CMR images for 5 random rats to compute the peak systolic strains and CL shear angles. Reproducibility of a given variable, X, was defined as the mean coefficient of variation (CoV) over the 5 rats as follows [16]:

$$CoV = \frac{\sum_{i=1}^{5}[St.Dev.(X_{Obs.1}X_{Obs.2})_i]}{\left|\sum_{i=1}^{5}[((X_{Obs.1}+X_{Obs.2})/2)_i]\right|}.$$

CoV ≤ 20% was considered reproducible.

Statistics

Strains and CL shear angles were represented as mean ± standard error of the mean (SEM). Multiple comparisons among the three regions (basal, mid-ventricle, and apical), among the three transmural layers in each wall segment, and among the four segments in each

transmural layer were conducted using One-Way ANOVA with post-hoc Bonferroni t-tests. A value of $p < 0.05$ was considered significant.

RESULTS

Distribution of peak systolic strains at base, mid-ventricle, and apex

The strain component E_{cc} exhibited similar peak systolic values at the base, mid-ventricle, and apex of rat LVs (Figure 3A). This trend was also seen in the E_{ll} and E_{rr} components. While the peak systolic shear strain components E_{rl} and E_{rc} assumed similar values at the three longitudinal LV levels, the peak systolic E_{cl} was significantly higher at the mid-ventricle compared to the apex (Figure 3B). It should be noted that maps of mid-ventricular end-systolic strain (E_{cc}, E_{ll}, and E_{cl}), from a representative animal, are shown in Figures 1E – 1G.

Distribution of peak systolic strain E_{cc} in the mid-ventricle

Within each transmural layer, E_{cc} assumed similar values in the four different wall segments, i.e., septal, inferior, lateral, and anterior segments, throughout the entire cardiac cycle (data not shown); there were no significant differences in the peak systolic values (Supplemental Figure 1A). However, peak systolic E_{cc} exhibited significant transmural differences in the entire mid-ventricular wall with the sub-endocardium shortening the most followed by the mid-myocardial and then sub-epicardial layers (Figure 4A). The strain-time curves separated during systole in the three transmural layers (Figure 4B).

Distribution of peak systolic strain E_{ll} in the mid-ventricle

In all four LV wall segments, peak systolic E_{ll} exhibited a uniform distribution across the three transmural layers (Supplemental Figure 1B). However, peak systolic E_{ll} varied significantly among the four LV wall segments with the maximum shortening occurring in the inferior region (Figure 5A). The strain-time curves for the four wall segments diverged during systole (Figure 5B).

Distribution of peak systolic strain E_{cl} in the mid-ventricle

There were significant differences in the peak systolic shear strain, E_{cl}, between the sub-epicardium and sub-endocardium in the inferior and anterior wall segments (Figure 6A). Moreover, peak systolic E_{cl} exhibited significant differences among the LV wall segments in both the sub-endocardial and mid-myocardial layers (Figure 6A). The strain-time curve obtained from the lateral wall showed that E_{cl} was effectively uniform across the three transmural layers throughout the entire cardiac cycle (Figures 6B).

Distributions of radial-related strain components (i.e., E_{rr}, E_{rl}, and E_{rc}) in the mid-ventricle

There was no significant difference observed in peak systolic E_{rr} among the four wall segments (Figure 7A); E_{rr} was uniformly distributed over the entire mid-LV slice throughout the entire cardiac cycle (Figure 7B). E_{rl} in the septal wall was smaller than strains in the lateral and anterior wall with significant differences detected for the peak values during

systole (Figure 8). The variations in E_{rc} were not associated with any statistical significance (Figure 9).

Distribution of ventricular torsion

Reflected as CL shear angle, peak ventricular torsion exhibited significant transmural differences between the sub-epicardium and sub-endocardium in the inferior and anterior wall segments (Figure 10A). Moreover, in the sub-endocardial and mid-myocardial layers, peak systolic torsion varied significantly among the four wall segments (Figure 10A). In the lateral wall segment, the ventricular torsion was uniform across the three transmural layers during the cardiac cycle (Figure 10B).

Reproducibility of 3D cardiac mechanics in rat LV

The reproducibility of the 6 strain components calculated over the entirety of each myocardial slice at the base, mid-ventricle, and apex was good with the exception of E_{cl} at the apex (Supplemental Table 1).

With smaller partitions in the mid-LV myocardium, the non-radial-related strains (i.e., E_{cc}, E_{ll}, and E_{cl}) were highly reproducible with CoV ≤ 15% in almost the entire myocardium, except that the CoV values of E_{ll} and E_{cl} in the anterior sub-endocardium ranged from 15% to 22%, which were considered borderline reproducible (Supplemental Figure 2). In terms of the radial-related strain components (i.e., E_{rr}, E_{rl}, and E_{rc}), although E_{rc} in the inferior wall segment exhibited poor reproducibility, the other strain components in the majority of the LV were reproducible (Supplemental Figure 3).

CL shear angle was reproducible over the entire myocardium (Supplemental Figure 4). In addition, the CoV values were lower than 15% in the septal, inferior, and lateral wall regardless of the transmural location.

DISCUSSION

The present study quantified the 3D Lagrangian strains in different regions in the LV wall of healthy rats and detected significant regional variations in systolic strains at the mid-ventricle. While the radial strain E_{rr} was uniformly distributed over the entire mid-ventricular myocardium, the other two normal components, E_{cc} and E_{ll}, exhibited significant differences along the transmural direction and among the wall segments, respectively. The observed transmural pattern of E_{cc} agrees with the reported results in murine models and humans [9, 23]. Moreover, both humans and rats exhibit higher E_{ll} in the inferior wall [24]. Interestingly, the distributions of shear strain, i.e., E_{cl}, E_{rc}, and E_{rl}, depended on their two respective components. In other words, E_{cl} varied in both the transmural direction and among wall segments, whereas E_{rl} only varied among the wall segments, and E_{rc} was not associated with any significant regional variations. The observed regional distributions of the 6 strain components may serve to coordinate the global LV deformation including radial thickening, circumferential and longitudinal shortening.

It should be noted that transmural distributions were not reported for the radial-related strain components (i.e., E_{rr}, E_{rl} and E_{rc}) in the present study. Notably, the measurement

of E_{rl} and E_{rc} was associated with large variabilities, which was also observed in murine models with 3D cine DENSE CMR [9]. Moreover, the radial-related strain components were less reproducible compared to the non-radial-related strains (i.e., E_{cc}, E_{ll}, and E_{cl}). Further partition in the thin transmural wall likely introduces more variability which resulted in poor reproducibility.

Torsion, as another important feature of LV deformation, was also assessed in the present study as CL shear angle. The overall trend of CL shear angle throughout the entire cardiac cycle was consistent with previously reported torsion time courses [9, 22]. As a result of heterogeneous contraction/shortening of myofibers in different regions, ventricular torsion also exhibited significant differences across the myocardium transmurally in some wall segments and varied among the wall segments particularly in the sub-endocardial and mid-myocardial layers. Accounting for different torsion definitions, the peak systolic torsion value averaged over the entire myocardium was consistent with those reported for rats [16], mice [9, 17] and humans [22]. With normalization to the radial and longitudinal distances, torsion calculated in the present study was highly reproducible overall.

One limitation of the present study was that we did not compare or relate the baseline observations in healthy rats to any disease conditions or treatments. However, a detailed profile of regional cardiac mechanics for healthy rats is necessary and can facilitate future extensive studies using rat models to study heart disease and treatments, especially because heart disease and/or treatments are associated with changes in specific myocardial regions [13–15]. Moreover, we did not include the strain analysis for the right ventricle (RV) in the present study. Since the RV is thin walled with a complex shape, the 3D strain analysis for RV may require acceleration techniques with higher resolution scans, which are still being developed. The tools for RV 3D DENSE analysis have only recently been developed [25]. Therefore, the 3D strain analysis of RV is beyond the scope of the current study and will be a focus of future work. In addition, only inter-observer reproducibility, not inter-test reproducibility, was assessed in the present study. However, cine DENSE CMR has been shown to have good inter-test reproducibility in mice [17], and we expect these findings to translate into rats. Finally, instead of the standard 6 LV wall segments used at the base and mid-ventricle, only 4 segments were assessed in order to increase the power to detect regional differences. In the current study, the ventricle was partitioned in the transmural direction, whereas the standard segments are composed of the full transmural thickness. Thus, it was necessary to increase the size to the segments, which is why 4 segments were employed.

CONCLUSIONS

During systole, the 3D Lagrangian strains, especially the E_{cc} and E_{ll} components, and ventricular torsion exhibit regional variation at the mid-ventricle of healthy rats. The results of the current study provide the necessary normative information of regional contractile function for rat hearts, which could facilitate further studies on changes induced by heart disease.

Supplementary Material

Refer to Web version on PubMed Central for supplementary material.

ACKNOWLEDGEMENTS

The authors wish to thank Hua Wang and Amir Nikou for their help with CMR scans. This study was supported by an award from the American Heart Association (14BGIA18850020), a grant from the National Science Foundation (CMMI-1538754), and grants from the National Institutes of Health (S10RR029541, P20GM103527, UL1TR000117).

LIST OF NON-STANDARD ABBREVIATIONS

CL	circumferential-longitudinal
CoV	coefficient of variation
ED	end diastole
Endo	sub-endocardium
Epi	sub-epicardium
ES	end systole
LV	left ventricle
Mid	mid-myocardium

REFERENCES

1. Goldman S and Raya TE, Rat infarct model of myocardial infarction and heart failure. J Card Fail, 1995. 1(2): p. 169–77. [PubMed: 9420647]
2. Patten RD and Hall-Porter MR, Small animal models of heart failure: development of novel therapies, past and present. Circ Heart Fail, 2009. 2(2): p. 138–44. [PubMed: 19808329]
3. Fomovsky GM and Holmes JW, Evolution of scar structure, mechanics, and ventricular function after myocardial infarction in the rat. Am J Physiol Heart Circ Physiol, 2010. 298(1): p. H221–8. [PubMed: 19897714]
4. Glukhov AV, Fedorov VV, Lou Q, Ravikumar VK, Kalish PW, Schuessler RB, Moazami N, and Efimov IR, Transmural dispersion of repolarization in failing and nonfailing human ventricle. Circ Res, 2010. 106(5): p. 981–91. [PubMed: 20093630]
5. Antzelevitch C, Sicouri S, Litovsky SH, Lukas A, Krishnan SC, Di Diego JM, Gintant GA, and Liu DW, Heterogeneity within the ventricular wall. Electrophysiology and pharmacology of epicardial, endocardial, and M cells. Circ Res, 1991. 69(6): p. 1427–49. [PubMed: 1659499]
6. Campbell SG, Haynes P, Kelsey Snapp W, Nava KE, and Campbell KS, Altered ventricular torsion and transmural patterns of myocyte relaxation precede heart failure in aging F344 rats. Am J Physiol Heart Circ Physiol, 2013. 305(5): p. H676–86. [PubMed: 23792678]
7. Kramer SP, Powell DK, Haggerty CM, Binkley CM, Mattingly AC, Cassis LA, Epstein FH, and Fornwalt BK, Obesity reduces left ventricular strains, torsion, and synchrony in mouse models: a cine displacement encoding with stimulated echoes (DENSE) cardiovascular magnetic resonance study. J Cardiovasc Magn Reson, 2013. 15: p. 109. [PubMed: 24380567]
8. Grothues F, Smith GC, Moon JC, Bellenger NG, Collins P, Klein HU, and Pennell DJ, Comparison of interstudy reproducibility of cardiovascular magnetic resonance with two-dimensional echocardiography in normal subjects and in patients with heart failure or left ventricular hypertrophy. Am J Cardiol, 2002. 90(1): p. 29–34. [PubMed: 12088775]

9. Zhong X, Gibberman LB, Spottiswoode BS, Gilliam AD, Meyer CH, French BA, and Epstein FH, Comprehensive cardiovascular magnetic resonance of myocardial mechanics in mice using three-dimensional cine DENSE. J Cardiovasc Magn Reson, 2011. 13: p. 83. [PubMed: 22208954]
10. Zerhouni EA, Parish DM, Rogers WJ, Yang A, and Shapiro EP, Human heart: tagging with MR imaging--a method for noninvasive assessment of myocardial motion. Radiology, 1988. 169(1): p. 59–63. [PubMed: 3420283]
11. Osman NF, Kerwin WS, McVeigh ER, and Prince JL, Cardiac motion tracking using CINE harmonic phase (HARP) magnetic resonance imaging. Magn Reson Med, 1999. 42(6): p. 1048–60. [PubMed: 10571926]
12. van Dijk P, Direct cardiac NMR imaging of heart wall and blood flow velocity. J Comput Assist Tomogr, 1984. 8(3): p. 429–36. [PubMed: 6725689]
13. Kim D, Gilson WD, Kramer CM, and Epstein FH, Myocardial tissue tracking with two-dimensional cine displacement-encoded MR imaging: development and initial evaluation. Radiology, 2004. 230(3): p. 862–71. [PubMed: 14739307]
14. Aletras AH, Ding S, Balaban RS, and Wen H, DENSE: displacement encoding with stimulated echoes in cardiac functional MRI. J Magn Reson, 1999. 137(1): p. 247–52. [PubMed: 10053155]
15. Liu W, Chen J, Ji S, Allen JS, Bayly PV, Wickline SA, and Yu X, Harmonic phase MR tagging for direct quantification of Lagrangian strain in rat hearts after myocardial infarction. Magn Reson Med, 2004. 52(6): p. 1282–90. [PubMed: 15562486]
16. Chen Y, Somji A, Yu X, and Stelzer JE, Altered in vivo left ventricular torsion and principal strains in hypothyroid rats. Am J Physiol Heart Circ Physiol, 2010. 299(5): p. H1577–87. [PubMed: 20729398]
17. Haggerty CM, Kramer SP, Binkley CM, Powell DK, Mattingly AC, Charnigo R, Epstein FH, and Fornwalt BK, Reproducibility of cine displacement encoding with stimulated echoes (DENSE) cardiovascular magnetic resonance for measuring left ventricular strains, torsion, and synchrony in mice. J Cardiovasc Magn Reson, 2013. 15: p. 71. [PubMed: 23981339]
18. Zhong X, Helm PA, and Epstein FH, Balanced multipoint displacement encoding for DENSE MRI. Magn Reson Med, 2009. 61(4): p. 981–8. [PubMed: 19189288]
19. Gilliam AD and Suever JD, DENSEanalysis. 2016: https://github.com/denseanalysis/denseanalysis.
20. Spottiswoode BS, Zhong X, Hess AT, Kramer CM, Meintjes EM, Mayosi BM, and Epstein FH, Tracking myocardial motion from cine DENSE images using spatiotemporal phase unwrapping and temporal fitting. IEEE Trans Med Imaging, 2007. 26(1): p. 15–30. [PubMed: 17243581]
21. Spottiswoode BS, Zhong X, Lorenz CH, Mayosi BM, Meintjes EM, and Epstein FH, Motion-guided segmentation for cine DENSE MRI. Med Image Anal, 2009. 13(1): p. 105–15. [PubMed: 18706851]
22. Russel IK, Tecelao SR, Kuijer JP, Heethaar RM, and Marcus JT, Comparison of 2D and 3D calculation of left ventricular torsion as circumferential-longitudinal shear angle using cardiovascular magnetic resonance tagging. J Cardiovasc Magn Reson, 2009. 11: p. 8. [PubMed: 19379480]
23. Zhong X, Spottiswoode BS, Meyer CH, Kramer CM, and Epstein FH, Imaging three-dimensional myocardial mechanics using navigator-gated volumetric spiral cine DENSE MRI. Magn Reson Med, 2010. 64(4): p. 1089–97. [PubMed: 20574967]
24. Marwick TH, Leano RL, Brown J, Sun JP, Hoffmann R, Lysyansky P, Becker M, and Thomas JD, Myocardial strain measurement with 2-dimensional speckle-tracking echocardiography: definition of normal range. JACC Cardiovasc Imaging, 2009. 2(1): p. 80–4. [PubMed: 19356538]
25. Suever J, Wehner G, Jing L, Powell D, Hamlet S, Grabau J, Mojsejenko D, Andres K, Haggerty C, and Fornwalt B, Right Ventricular Strain, Torsion, and Dyssynchrony in Healthy Subjects using 3D Spiral Cine DENSE Magnetic Resonance Imaging. IEEE Trans Med Imaging, 2016.

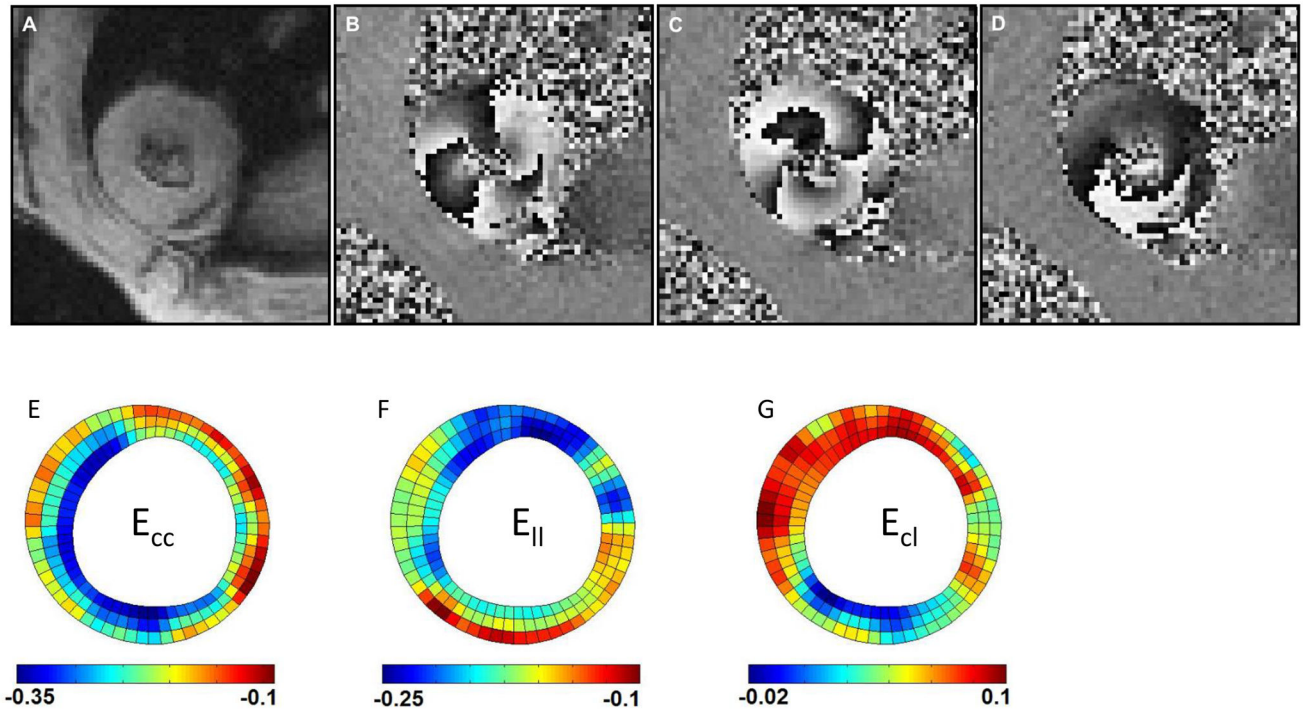

Figure 1. Representative end-systolic 3D cine DENSE CMR images and end-systolic strain maps from one mid-ventricular short-axis slice of a rat left ventricle.

(A) A magnitude-reconstructed image; (B) a phase image encoded for x-displacement; (C) a phase image encoded for y-displacement; (D) a phase image encoded for z-displacement; (E) example of E_{cc} strain distribution; (F) example of E_{ll} strain distribution; (G) example of E_{cl} strain distribution. Note: Panels (E), (F), and (G) each have their own distinct scale bar.

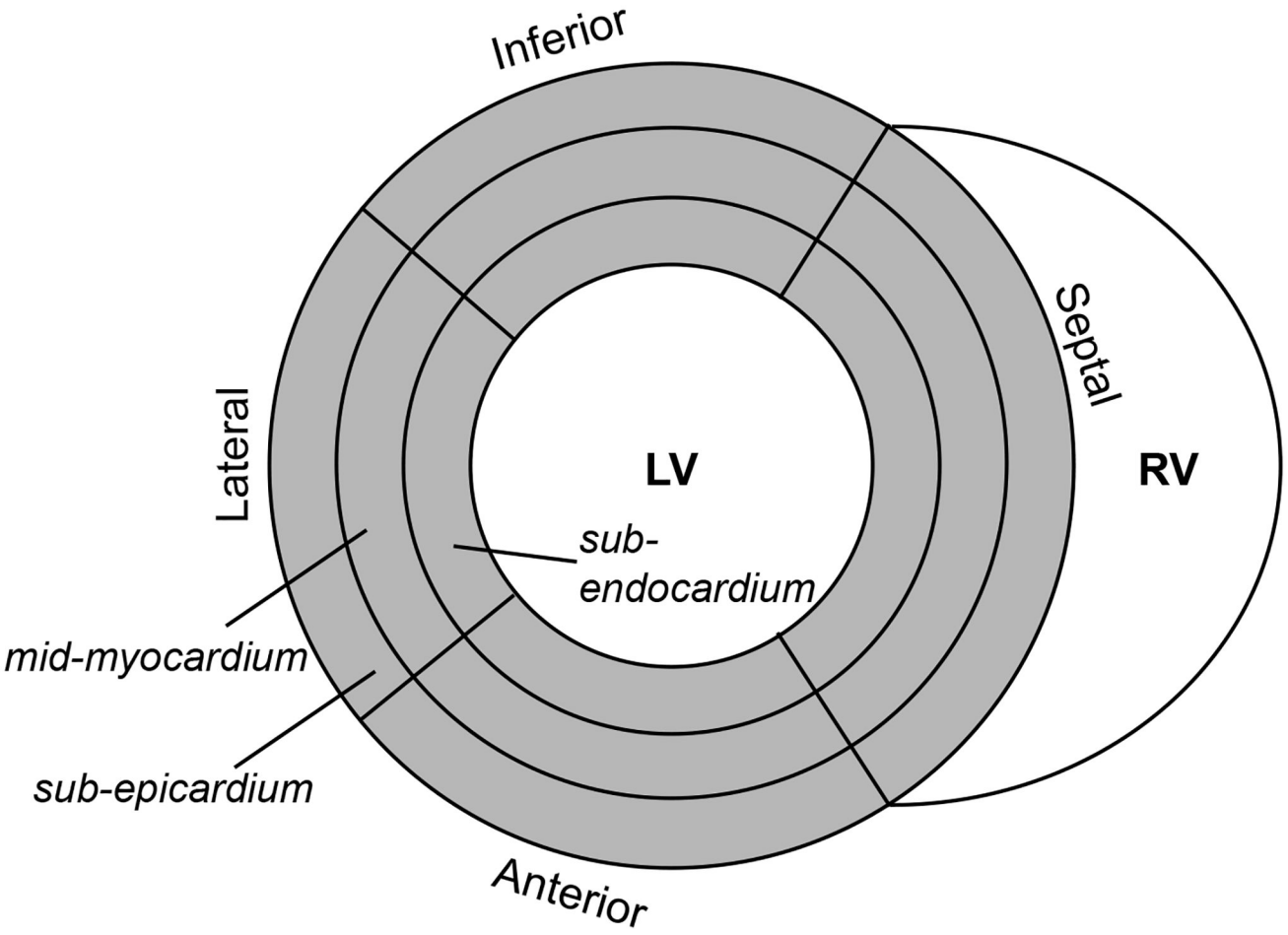

Figure 2.
Diagram of mid-ventricular myocardial segmentation.

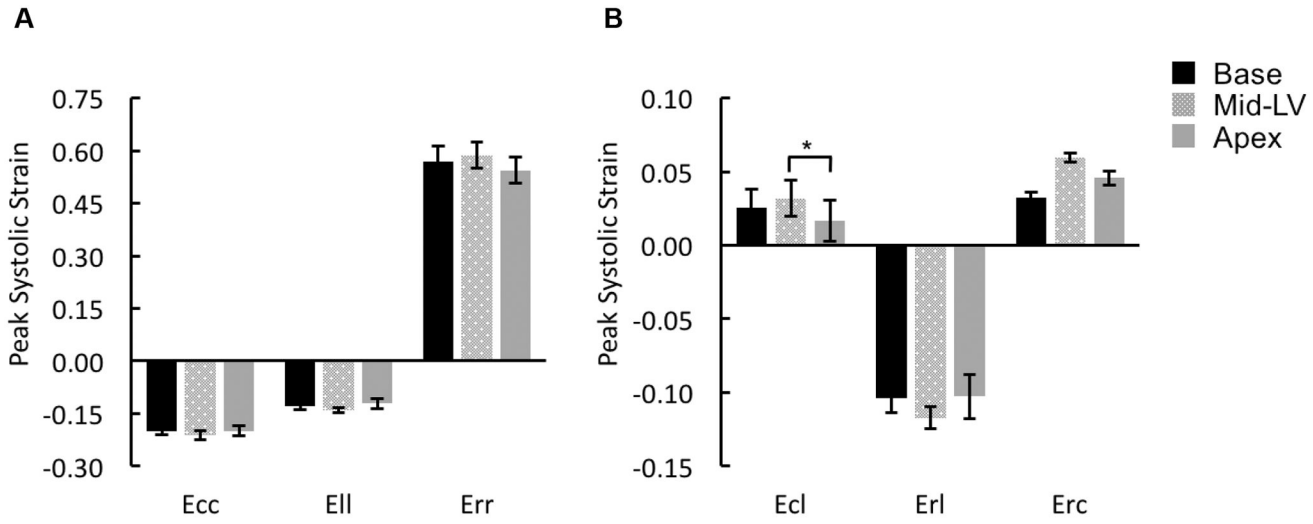

Figure 3. Distributions of peak systolic strains at base, mid-ventricle, and apex.

Peak systolic strains for normal components (A: E_{cc}, E_{ll}, and E_{rr}) and shear components (B: E_{cl}, E_{rl}, and E_{rc}) were averaged over the entire slice at either basal [Base], mid-ventricular [Mid-LV], or apical [Apex] level of rat LVs. *$p < 0.05$.

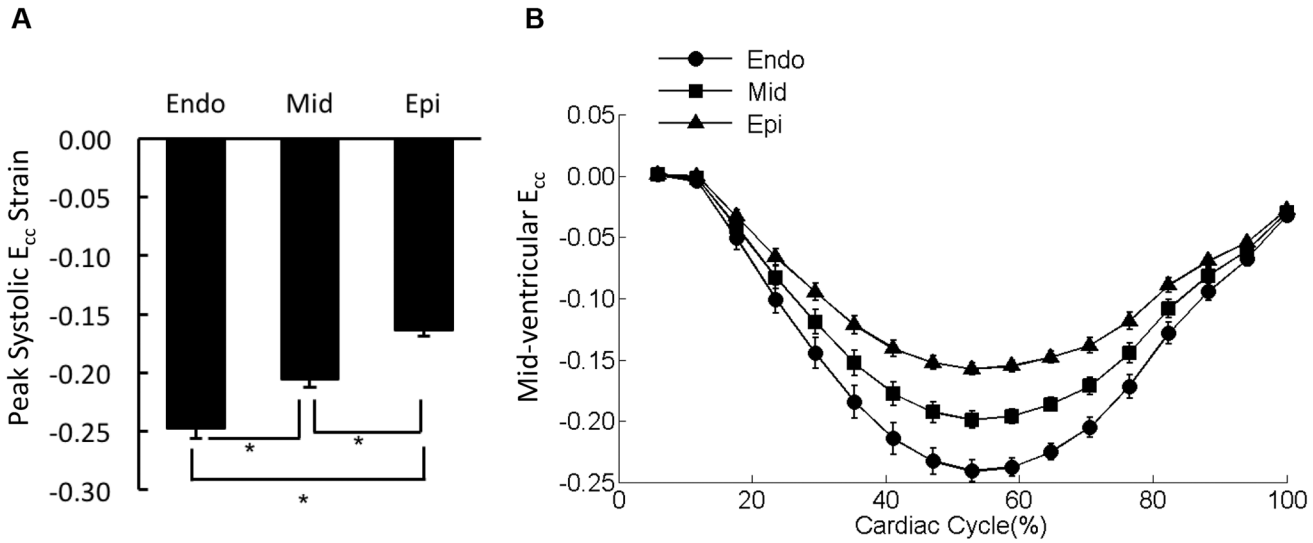

Figure 4. Distribution of E_{cc} in the mid-ventricle.

(A) The peak systolic E_{cc} values were averaged over each of the three transmural layers of the mid-ventricular slice (sub-endocardium [Endo], mid-myocardium [Mid], and sub-epicardium [Epi]). *$p < 0.05$. (B) The strain-time curves for E_{cc} in the three transmural layers of mid-ventricular slice were overlaid. Cardiac cycle started with end diastolic state.

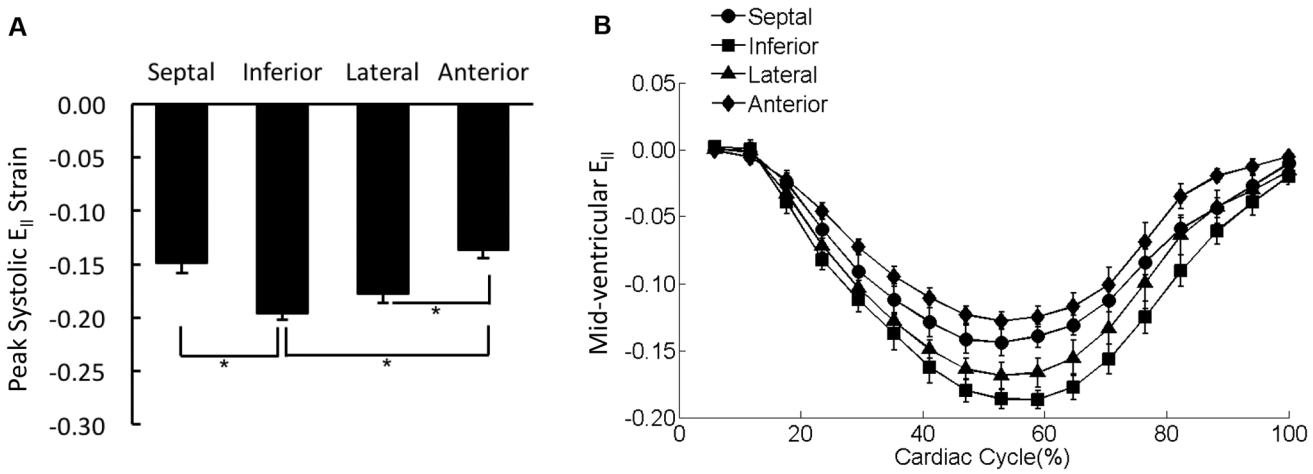

Figure 5. Distribution of E_{ll} in the mid-ventricle.

(A) The peak systolic E_{ll} values were averaged over each of the four wall segments of the mid-ventricular slice regardless the transmural location. *$p < 0.05$. (B) The strain-time curves for E_{ll} in the four wall segments of mid-ventricular slice were overlaid. Cardiac cycle started with end diastolic state.

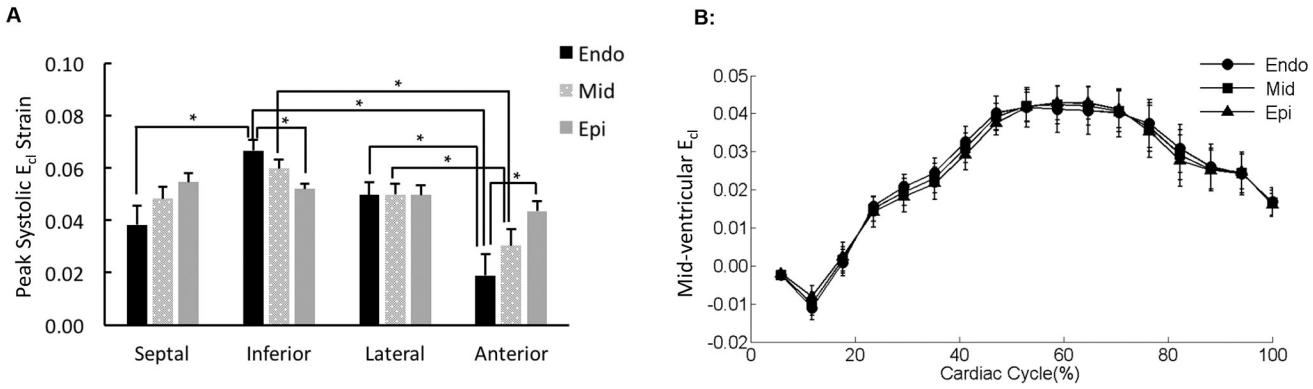

Figure 6. Distribution of E_{cl} in the mid-ventricle.

(A) The peak systolic E_{cl} values were averaged over each region of the mid-ventricular slice (sub-endocardium [Endo], mid-myocardium [Mid], and sub-epicardium [Epi]). *$p < 0.05$. (B) The strain-time curves for E_{cl} in the three transmural layers of the representative lateral mid-ventricular wall were overlaid. Cardiac cycle started with end diastolic state.

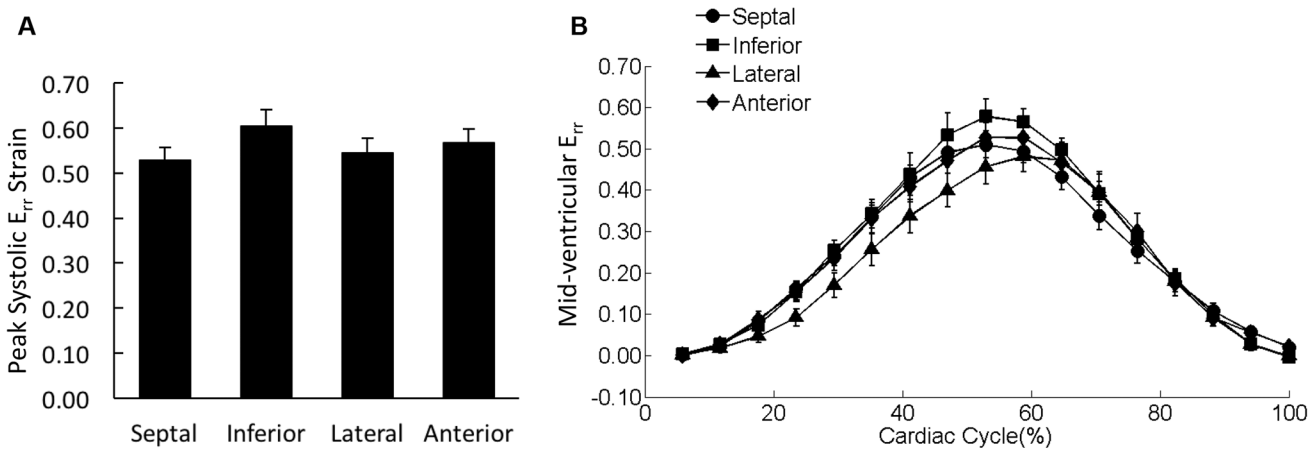

Figure 7. Distribution of E_{rr} in the mid-ventricle.

(A) The peak systolic E_{rr} values were averaged over each of the four wall segments of the mid-ventricular slice regardless the transmural location. (B) The strain-time curves for E_{rr} in the four wall segments of mid-ventricular slice were overlaid. Cardiac cycle started with end diastolic state.

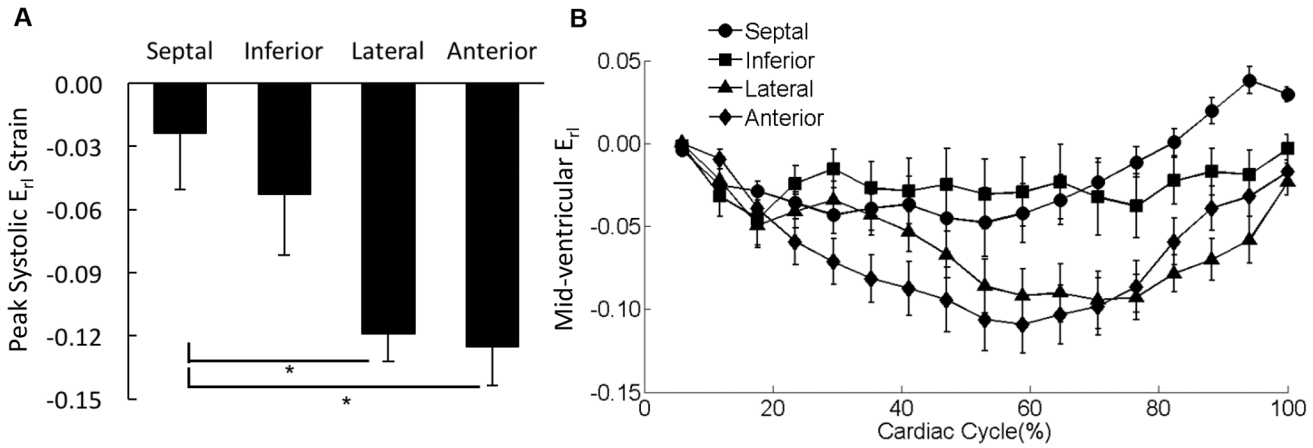

Figure 8. Distribution of E_{rl} in the mid-ventricle.

(A) The peak systolic E_{rl} values were averaged over each of the four wall segments of the mid-ventricular slice regardless the transmural location. *$p < 0.05$. (B) The strain-time curves for E_{rl} in the four wall segments of mid-ventricular slice were overlaid. Cardiac cycle started with end diastolic state.

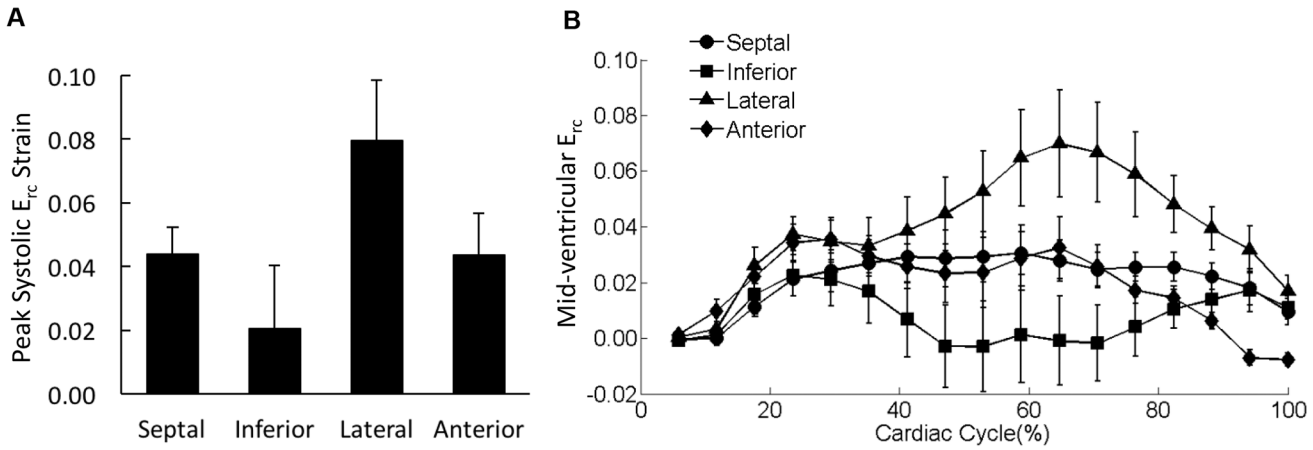

Figure 9. Distribution of E_{rc} in the mid-ventricle.

(A) The peak systolic E_{rc} values were averaged over each of the four wall segments of the mid-ventricular slice regardless the transmural location. (B) The strain-time curves for E_{rc} in the four wall segments of mid-ventricular slice were overlaid. Cardiac cycle started with end diastolic state.

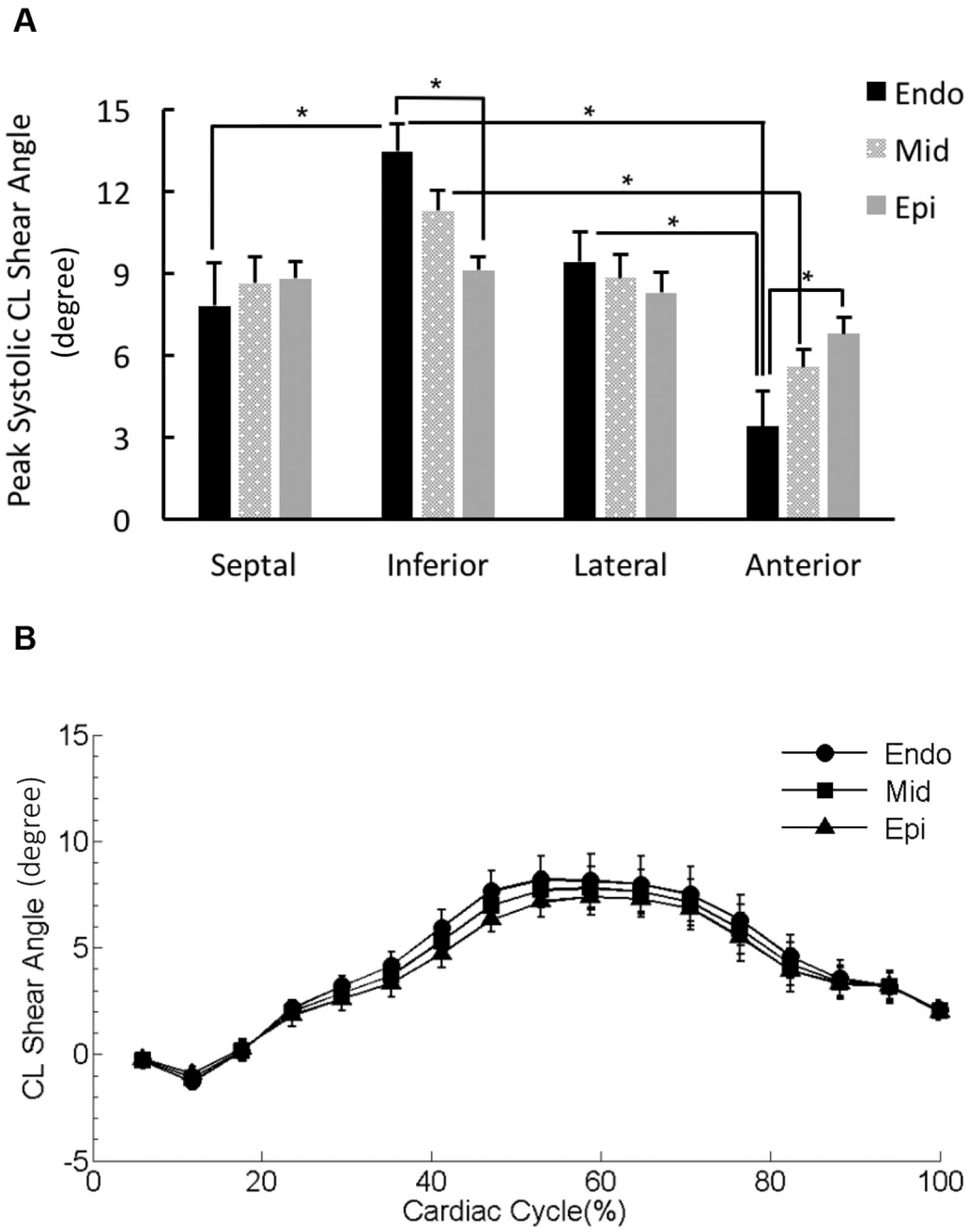

Figure 10. Regional ventricular torsion.

(A) Peak ventricular torsion was presented as peak circumferential-longitudinal (CL) shear angle and calculated for the three transmural layers (sub-endocardium [Endo], mid-myocardium [Mid], and sub-epicardium [Epi]) in the four wall segments. *$p < 0.05$. (B) The CL shear angle-time curves for the three transmural layers in the representative lateral wall segment were overlaid. Cardiac cycle started with end diastolic state.